

Ag₂Ti₂P₂S₁₁: A New Layered Thiophosphate. Synthesis, Structure Determination and Temperature Dependence of the Silver Distribution

E. GAUDIN,^a L. FISCHER,^a F. BOUCHER,^a M. EVAIN^{a*} AND V. PETRICEK^b

^aLaboratoire de Chimie des Solides, IMN, UMR CNRS No. 110, Université de Nantes, 2 rue de la Houssinière, 44072 Nantes CEDEX 03, France, and ^bInstitute of Physics, Academy of Sciences of the Czech Republic, Na Slovance 2, 180 40 Praha 8, Czech Republic. E-mail: evain@cnrs-umn.fr

(Received 6 May 1996; accepted 6 September 1996)

Abstract

The new Ag₂Ti₂P₂S₁₁ quaternary phosphosulfide disilver dititanium undecathiodiphosphate is obtained by heating the elements at *ca* 850 K in an evacuated silica tube. It crystallizes in orthorhombic symmetry, *Pnma* space group, with *a* = 8.5222 (11), *b* = 6.8359 (10), *c* = 24.142 (4) Å, *V* = 1406.4 (4) Å³ and *Z* = 4 at 293 K. The refinement of the room-temperature structure leads to a reliability factor of *R* = 0.0378 for 1556 independent reflections and 128 variables. Ag₂Ti₂P₂S₁₁ is composed of layers, separated by van der Waals gaps. The layers are composed of [Ti₂S₉] chains built from [TiS₇] units (TiS₆ octahedra in which a corner has been replaced by an S₂ pair) and linked through regular [PS₄] and highly distorted [AgS₄] tetrahedra. The formula of the compound can be written as Ag₂^ITi₂^{IV}P₂^V(S₂)^{-II}S₉^{-II}. A Gram-Charlier anharmonic development of the atomic displacement factor for Ag atoms reveals a strong non-harmonic probability density deformation, especially in the direction of two empty neighbouring tetrahedra, away from the Ti and P cations. The temperature dependence of the effective one-particle potential shows that the Ag distribution is primarily static in nature. At high temperature the tetrahedrally coordinated site is the preferential site. At lower temperature the Ag atoms are redistributed over the tetrahedral site and the adjacent triangular site. The disorder could not be resolved due to a phase transition with splitting of spots just below room temperature.

1. Introduction

In the M₂P₂S₆ family, first discovered by Friedel (1894), characterized by Klingen, Eulenberger & Hahn (1968) and then extensively studied by several authors (Brec, 1986, and references therein), the stability of the transition metal in its +II oxidation state decreases from Zn to Ti. Indeed, the *M d*-orbital energy levels ascend progressively, favouring a higher oxidation state through a depletion of the

uppermost filled levels. In the vanadium case, for instance, 'V₂P₂S₆' does not exist, but a mixed-valence phase V_{0.44}^{III}V_{0.34}^{IV}[]_{0.22}PS₃ is found instead (Ouvrard, Fréour, Brec & Rouxel, 1985). The vanadium higher oxidation state V^{III} can be isolated when one half of the vanadium potential amount is substituted by M^I cations. Phases such as AgVP₂S₆ (Lee, Colombet, Ouvrard & Brec, 1986), AgVP₂Se₆ (Ouvrard & Brec, 1988) or CuVP₂S₆ (Durand, Ouvrard, Evain & Brec, 1990) are thus obtained with Ag^I or Cu^I, whereas different stoichiometries are observed with larger cations [*e.g.* RbVP₂S₇ (Durand, Evain & Brec, 1993)]. Beyond vanadium, the M₂P₂S₆ structural model is no longer possible and titanium is present as Ti^{IV} in TiP₂S₆ (Jandali, Eulenberger & Hahn, 1980) and Ti₄P₈S₂₉ (Jandali, Eulenberger & Hahn, 1985), which present different structural patterns. To stabilize titanium oxidation states other than IV, we decided to investigate the Ag-Ti-P-S system.

The choice of silver as the M^I counter-cation was twofold. On the one hand, AgVP₂X₆ phases had already been obtained (*vide supra*). On the other hand, *d*¹⁰ cations are known to exhibit interesting specific characteristics, *e.g.* abnormally high atomic displacement parameters (ADP's), a preference for low coordination environments and a tendency to form *d*¹⁰-*d*¹⁰ homoatomic bonds when their concentration is large (Jansen, 1987, and references therein). In the last decade, a particular interest has been devoted to the former characteristic, *i.e.* the high ADP's, and the deformation of the electronic distribution. Such a deformation can be explained either by a positional disorder (see for instance van der Lee, Boucher, Evain & Brec, 1993) or by anharmonic thermal vibrations (Yoshiasa, Koto, Kanamaru, Emura & Horiuchi, 1987). Several detailed spectroscopic and crystallographic studies (Barj, Lucazeau, Ouvrard & Brec, 1988; Boucher, Evain & Brec, 1994) have clearly demonstrated that for the *d*¹⁰ cations the unusually large ADP's resulted from a static disorder generated by several off-centre displacements of the

Table 1. *Experimental details*

Crystal data	293	348	398	448
Temperature (K)	293	348	398	448
Chemical formula			$\text{Ag}_2\text{Ti}_2\text{P}_2\text{S}_{11}$	
Chemical formula weight			726.14	
Space group			$Pnma$ (62)	
a (Å)	8.5222 (11)	8.530 (2)	8.533 (2)	8.536 (3)
b (Å)	6.8359 (10)	6.848 (4)	6.851 (5)	6.855 (6)
c (Å)	24.142 (4)	24.171 (6)	24.198 (9)	24.22 (11)
V (Å ³) ($Z = 4$)	1406.4 (4)	1411.8 (9)	1414.6 (12)	1417.4 (14)
D_x (Mg m ⁻³)	3.428	3.416	3.410	3.403
Crystal form			Thick elongated platelets	
Crystal size (mm ³)	0.014 × 0.050 × 0.23		0.015 × 0.11 × 0.25	
Crystal colour			Black	
$F(000)$			1376	
Data collection				
Diffractometer		Enraf-Nonius CAD-4		
Radiation		Mo $K\text{-}L_{2,3}$ (0.71073 Å)		
Monochromator		Oriented graphite (002)		
Scan mode		$\omega\text{-}\theta$		
Recording range θ (°)		1–35		
Range of h, k, l	$-1 \rightarrow h \rightarrow 13$		$-1 \rightarrow h \rightarrow 13$	
	$-1 \rightarrow k \rightarrow 11$		$-1 \rightarrow k \rightarrow 11$	
	$-1 \rightarrow l \rightarrow 38$		$-1 \rightarrow l \rightarrow 39$	
Standard reflections (every h)	022, 022, 218		204, 218, 24, 10	
Intensity decay (%)	< 0.5	1.2	3.1	9.1
Reflections for crystal matrix orientation ($8 < \theta < 16^\circ$)	24		25	
Data reduction				
No. of recorded reflections	4525	4543	4547	4555
No. of independent reflections	2482	2292	2335	2255
Absorption correction			Gaussian method	
Linear absorption coefficient (cm ⁻¹)	56.6	56.4	56.3	56.2
T_{\min}	0.762	0.556	0.556	0.551
T_{\max}	0.924	0.916	0.916	0.916
No. of independent reflections with $I > 3.0\sigma(I)$ (N)	1556	1502	1523	1363
$R_{\text{int}} = \Sigma I - I_{\text{av}} /\Sigma I$ (%) for observed reflections	2.61	2.21	2.42	2.51
Refinement*				
Weighting scheme		$w = 1/[\sigma^2 F_o + (0.011 F_o)^2]$		
R (%)	3.78	3.54	3.99	3.90
wR (%)	3.85	3.63	4.95	3.78
S	1.28	1.54	2.02	1.52
Refined parameters (M)			128	
$(\Delta/\sigma)_{\max}$			< 0.001	
Extinction coefficient	0.41 (2)	0.168 (11)	0.099 (12)	0.069 (9)
Difference Fourier residues (e Å ⁻³)	[-1.67, +1.16]	[-0.92, +1.00]	[-1.34, +1.41]	[-0.93, +1.06]

* $R = \Sigma||F_o| - |F_c||/\Sigma|F_o|$. $wR = [\Sigma w(|F_o| - |F_c|)^2/\Sigma w|F_o|^2]^{1/2}$. $S = [\Sigma w(|F_o| - |F_c|)^2/(N - M)]^{1/2}$. Isotropic secondary extinction - Type I - Gaussian distribution (Becker & Coppens, 1974).

cations. These displacements were demonstrated to arise from second-order Jahn-Teller effects (Burdett & Eisenstein, 1992), initially thought to always involve the filled d orbitals (Boucher, 1993). It was later shown that other mechanisms are also possible when those orbitals are too low in energy (Zhukov, Boucher, Alemany, Evain & Alvarez, 1995).

In that investigation of the Ag-Ti-P-S system a new phosphosulfide, $\text{Ag}_2\text{Ti}_2\text{P}_2\text{S}_{11}$, was obtained. In this paper we report its synthesis and structure determination and we analyse the silver ADP's as a function of temperature.

2. Experimental

2.1. Synthesis

$\text{Ag}_2\text{Ti}_2\text{P}_2\text{S}_{11}$ was obtained from heating the constituent elements in a stoichiometric proportion (2:2:2:11) in an evacuated silica tube. The mixture was maintained at a temperature of 873 K for 10 d and then cooled to room temperature at 50 K h⁻¹. As no well shaped single crystals were obtained, the product was ground under nitrogen atmosphere, heated again at 848 K for a week and finally annealed for 3 d at 698 K.

This synthesis led to two different types of crystals: needle-shaped crystals with a hexagonal section which were identified as $\text{AgTi}_2\text{P}_3\text{S}_{12}$ (Cieren, Angenault, Couturier & Quarton, 1995) and platelet-shaped crystals which correspond to the title compound. A semi-quantitative analysis on those latter crystals by means of a JEOL microscope (TRACOR-TN 5500 equipped JEOL-JSM35C) confirmed the $\text{Ag}_2\text{Ti}_2\text{P}_2\text{S}_{11}$ stoichiometry. A mixture of the two phases could not be prevented.

2.2. Data collection

A good quality single crystal of proper shape was selected and tested by the usual rotation and Weissenberg techniques. In this preliminary study an orthorhombic lattice cell with the parameters $a \approx 8.5$, $b \approx 6.8$ and $c \approx 12.1$ Å was observed. In addition, a sublattice of weaker spots could be identified corresponding to a twofold superstructure along the c axis. The chosen crystal was glued to the tip of a Lindemann quartz capillary using a Torr Seal vacuum sealing kit. The diffracted intensities were collected at four different temperatures (293, 348, 398 and 448 K) on an Enraf-Nonius CAD4-F diffractometer equipped with an AET hot-gas (nitrogen) blowing apparatus. Mo $K\text{-}L_{2,3}$ radiation and a graphite monochromator were used. The preliminary cell-parameter assignment was confirmed with $a = 8.5222(11)$, $b = 6.8359(10)$, $c = 24.142(4)$ Å and $V = 1406.4(4)$ Å³ at room temperature. As the single crystal used for the room-temperature data collection was lost after the measurement, a second one was selected for the temperature analyses. To minimize expansion effect, the high-temperature data collections were performed in an azimuthal mode with a 20° psi value. Data collection above 448 K could not be completed because of crystal deterioration. The detailed recording conditions are reported in Table 1.

2.3. Data processing

In the data reduction reflections with either an asymmetric background (BG left/BG right \neq [1/3,3]) or a deviated position were rejected. The measured intensities were corrected for scale variation based upon standards and Lorentz and polarization effects. A Gaussian-type absorption correction was then applied with the *Xtal3.4* system (Hall, King & Stewart, 1995). An optimization of the thickness of both crystals was carried out using the refinement reliability factors. Symmetry-related reflections were averaged according to the *mmm* Laue symmetry. All refinements were carried out with the *SDS95* program package (Petricek, 1995) that provides calculations for non-harmonic atomic displacement parameters. A Gram-Charlier expansion up to the fifth order (Johnson & Levy, 1974) was used for the Ag atoms. The scattering factors for neutral atoms and the correction terms for

anomalous dispersion were taken from Cromer & Waber (1974) and Cromer (1974), respectively. The atomic parameters, scale factors and isotropic extinction coefficients (Becker & Coppens, 1974) were refined in a full matrix mode, minimizing the function $wR = [\sum w(|F_o| - |F_c|)^2 / \sum w F_o^2]^{1/2}$. A weighting scheme based on $\sigma(F_o)$, corrected with an instability coefficient (see Table 1), was used.

2.4. Structure refinement

The initial refinement was performed on the room-temperature data set with the main reflections only, *i.e.* without any superstructure spots. The non-conventional space group *Pbma* was found to be compatible with the observed extinction rules. Several atoms were then located with the *SHELXTL-Plus*TM (Sheldrick, 1991) direct-methods program and the remaining atom positions were determined from difference-Fourier maps and structure visualization. This solution already accounted for most of the structural features, apart from the ordering of three S atoms (half occupied positions) within the titanium coordination sphere (*vide infra*).

The atomic position list of the average cell was then expanded to the supercell. Following the *International*

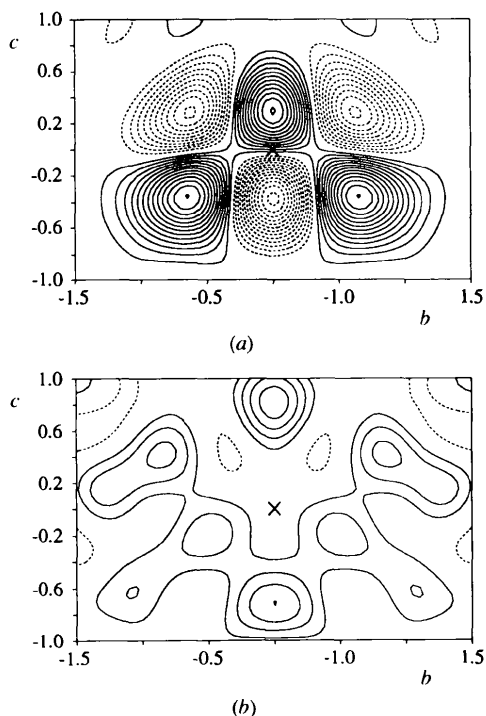


Fig. 1. Difference-Fourier maps (Å) around the Ag1 mean position for $\text{Ag}_2\text{Ti}_2\text{P}_2\text{S}_{11}$ (293 K): (a) harmonic refinement; (b) non-harmonic refinement. Both yz sections at $x = 0.3960$. The Ag1 mean position is indicated by \times . (a) Contour lines from -6.5 to -0.5 (dashed lines) and from 0.5 to $6.5 e^{-3}$ (continuous lines) in intervals of $0.5 e^{-3}$; (b) contour lines at -0.2 (dashed lines) and from 0.2 to $0.8 e^{-3}$ (continuous lines) in intervals of $0.2 e^{-3}$.

Tables for X-ray Crystallography (1974, Vol. IV), and in agreement with the extinction conditions, *Pnma* was selected as a possible space group. Given the various possibilities for the choice of origin, the resolution was first attempted in the *P1* space group. The occupation ratios of the partially occupied sulfur positions were

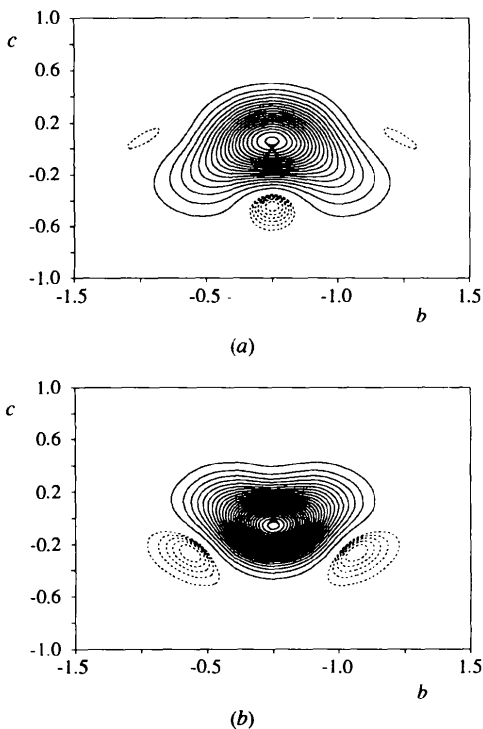


Fig. 2. Non-harmonic p.d.f. maps (\AA^{-3}) of silver for $\text{Ag}_2\text{Ti}_2\text{P}_2\text{S}_{11}$ (293 K): (a) Ag1; yz sections at $x = 0.3960$; contour lines from -300 to -50\AA^{-3} in intervals of 50\AA^{-3} (dashed lines) and from 500 to 9500\AA^{-3} in intervals of 500\AA^{-3} (continuous lines); (b) Ag2; yz sections at $x = 0.607$; contour lines from -250 to -50\AA^{-3} in intervals of 50\AA^{-3} (dashed lines) and from 500 to $13\,500 \text{\AA}^{-3}$ in intervals of 500\AA^{-3} (continuous lines). Ag mean positions indicated by \times .

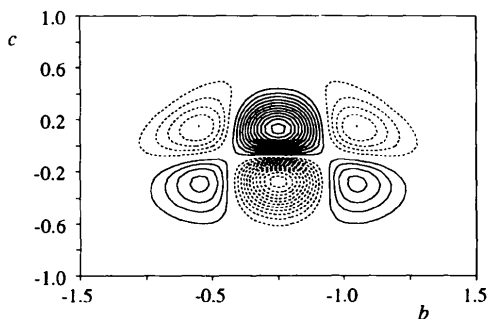


Fig. 3. Non-harmonic deformation-density map (\AA^{-3}) of Ag1 for $\text{Ag}_2\text{Ti}_2\text{P}_2\text{S}_{11}$ (293 K); yz sections at $x = 0.3960$; contour lines from -2400 to -200\AA^{-3} (dashed lines) and from 200 to 2400\AA^{-3} (continuous lines). Ag1 mean positions indicated by \times .

Table 2. Fractional atomic coordinates and equivalent isotropic displacement parameters (\AA^2)

$$B_{\text{eq}} = (8\pi^2/3) \sum_i \sum_j U^{ij} a_i^* a_j^* \mathbf{a}_i \cdot \mathbf{a}_j$$

	<i>x</i>	<i>y</i>	<i>z</i>	<i>B</i> _{eq}
Ag1	0.3960 (3)	1/4	0.30156 (10)	5.46 (8)
Ag2	0.6074 (2)	3/4	0.19497 (6)	3.36 (2)
Ti1	0.74486 (15)	0.00434 (14)	0.42200 (3)	0.76 (2)
P1	0.0029 (2)	1/4	0.35015 (8)	0.81 (4)
P2	0.0017 (2)	3/4	0.15150 (8)	0.84 (4)
S1	0.1102 (3)	1/4	0.27591 (9)	1.55 (6)
S2	0.8946 (2)	3/4	0.22563 (8)	1.59 (6)
S3	0.9605 (2)	0.9957 (2)	0.10589 (7)	1.10 (4)
S4	0.0411 (2)	0.9975 (2)	0.39329 (7)	1.06 (4)
S5	0.7598 (2)	1/4	0.34353 (7)	0.82 (4)
S6	0.2442 (2)	3/4	0.15469 (7)	0.85 (4)
S7	0.6199 (2)	1/4	0.48251 (7)	1.06 (4)
S8	0.8585 (2)	1/4	0.48469 (8)	1.07 (4)
S9	0.7598 (2)	3/4	0.48494 (7)	1.11 (3)

refined and a damping factor was used to reach convergence. Finally, by simply removing the sulfur positions with a non-significant occupancy factor, a final ordered model was found. The symmetry elements of the *Pnma* space group were then found with the *BUNYIP* program of the *Xtal3.4* system (Hall, King & Stewart, 1995).

Hence, with 14 fully occupied independent positions, isotropic ADP's and no damping factor, the refinement converged to the confidence factors $R/wR = 0.148/0.181$ for 1556 reflections. Introducing anisotropic ADP's for all positions and an isotropic extinction coefficient, $R/wR = 0.0709/0.0796$ values were obtained. At this stage, a difference-Fourier map revealed significant residues around both silver sites ($\pm 6.5 \text{e \AA}^{-3}$, see Fig. 1a). For a better description of the electronic density around those sites, an expansion of the atomic displacement factor was introduced (Bachmann & Schulz, 1984). Gram-Charlier expansions (Johnson & Levy, 1974) up to the fifth order for Ag1 and the third order for Ag2 were used. Site-symmetry restrictions were applied on tensor components according to Kuhs (1984). Although many non-harmonic coefficients were non-significant at the end of the refinement, they were not fixed to zero because of a satisfactory ratio between the number of refined parameters (128) and the number of independent reflections (1556). With 33 additional parameters (with regard to the refinement with anisotropic ADP's) the reliability factors dropped smoothly to the values $R/wR = 0.0378/0.0385$ (see Table 1). No significant density was then found in the difference-Fourier map in the vicinity of the silver sites (see Fig. 1b).

In Figs. 2(a) and (b) are shown the most significant non-harmonic probability density function (p.d.f.) sections for Ag1 and Ag2, respectively. Considering the small negative regions, the refined model can be considered as valid (Bachmann &

Table 3. *Isotropic displacement parameters** ($T = 293\text{ K}$)

	U^{11}	U^{22}	U^{33}	U^{12}	U^{13}	U^{23}
Ag1	0.0205 (9)	0.141 (3)	0.0461 (12)	0	0.0008 (8)	0
Ag2	0.0207 (4)	0.0768 (8)	0.0303 (4)	0	-0.0023 (3)	0
Ti1	0.0098 (3)	0.0085 (3)	0.0106 (3)	0.0000 (3)	0.0005 (6)	0.0010 (4)
P1	0.0084 (8)	0.0109 (11)	0.0114 (8)	0	0.0002 (7)	0
P2	0.0095 (9)	0.0122 (11)	0.0101 (8)	0	0.0007 (7)	0
S1	0.0151 (11)	0.032 (2)	0.0115 (9)	0	0.0037 (8)	0
S2	0.0108 (10)	0.038 (2)	0.0116 (8)	0	0.0018 (8)	0
S3	0.0100 (6)	0.0133 (11)	0.0183 (9)	0.0011 (5)	-0.0004 (7)	0.0029 (5)
S4	0.0113 (6)	0.0110 (11)	0.0179 (9)	0.0019 (5)	0.0002 (7)	0.0024 (5)
S5	0.0089 (8)	0.0129 (9)	0.0094 (6)	0	-0.0003 (8)	0
S6	0.0099 (8)	0.0123 (9)	0.0102 (7)	0	-0.0023 (8)	0
S7	0.0122 (8)	0.0149 (10)	0.0131 (8)	0	0.0023 (6)	0
S8	0.0140 (8)	0.0133 (10)	0.0132 (8)	0	-0.0032 (6)	0
S9	0.0205 (9)	0.0114 (7)	0.0100 (6)	0	-0.0008 (7)	0

* Isotropic equivalent ADP's defined as: $B_{\text{eq}}(\text{\AA}^2) = \frac{1}{3}\text{trace}(\beta g)$ or $B_{\text{eq}} = (8\pi^2/3) \sum_i \sum_j U^{ij} a_i^* a_j^* a_i \cdot a_j$. The expression of the harmonic displacement factor is: $\exp(-2\pi^2 \sum_i \sum_j U^{ij} a_i^* a_j^* h_i h_j)$, with U^{ij} in \AA^2 .

Table 4. *Silver atomic displacement parameters*

T (K)	293		348		398		448	
	Ag1	Ag2	Ag1	Ag2	Ag1	Ag2	Ag1	Ag2
C_{111}	-0.03 (13)	-0.01 (4)	-0.24 (14)	-0.14 (5)	-0.3 (2)	-0.11 (7)	-0.5 (2)	-0.18 (8)
C_{113}	-0.02 (3)	0.011 (11)	0.00 (3)	0.006 (13)	0.03 (4)	0.01 (2)	0.02 (4)	0.02 (2)
C_{122}	-1.4 (3)	0.45 (8)	-1.1 (4)	0.56 (9)	-1.8 (5)	1.04 (15)	-2.6 (5)	1.36 (15)
C_{133}	-0.060 (11)	0.014 (4)	-0.044 (13)	0.022 (5)	-0.07 (2)	0.033 (7)	-0.10 (2)	0.027 (7)
C_{223}	-1.84 (12)	0.71 (3)	-2.12 (15)	1.00 (4)	-2.5 (2)	1.24 (6)	-2.9 (3)	1.53 (6)
C_{333}	-0.016 (8)	0.005 (2)	-0.012 (10)	0.011 (3)	-0.015 (15)	0.008 (4)	-0.015 (15)	0.012 (5)
D_{1111}^*	-0.01 (4)		-0.05 (4)		-0.03 (6)		-0.01 (7)	
D_{1113}	0.000 (8)		-0.011 (9)		-0.010 (15)		-0.03 (2)	
D_{1122}	0.09 (8)		0.33 (9)		0.34 (15)		0.7 (2)	
D_{1133}	0.002 (3)		0.003 (3)		0.005 (5)		0.013 (6)	
D_{1223}	0.10 (3)		0.14 (3)		0.28 (5)		0.33 (6)	
D_{1333}	-0.0015 (14)		-0.001 (2)		-0.003 (3)		-0.006 (4)	
D_{2222}	-0.5 (8)		-0.1 (11)		-2 (2)		-2 (2)	
D_{2233}	0.157 (15)		0.28 (2)		0.33 (3)		0.46 (4)	
D_{3333}	0.0001 (11)		0.005 (2)		0.004 (3)		0.004 (3)	
E_{11111}^*	0.00 (4)		-0.05 (5)		-0.03 (7)		-0.06 (7)	
E_{11113}	-0.004 (7)		0.004 (8)		0.005 (14)		0.006 (15)	
E_{11122}	0.09 (6)		0.12 (8)		0.04 (12)		-0.13 (14)	
E_{11133}	-0.003 (2)		-0.001 (3)		-0.004 (5)		-0.002 (5)	
E_{11223}	-0.030 (15)		-0.06 (2)		-0.08 (3)		-0.10 (4)	
E_{11333}	0.0006 (8)		0.0000 (11)		0.001 (2)		0.001 (2)	
E_{12222}	0.0 (4)		1.7 (5)		1.1 (9)		2 (1)	
E_{12233}	-0.006 (6)		-0.001 (8)		-0.001 (14)		0.00 (2)	
E_{13333}	-0.0004 (5)		0.0005 (7)		0.0007 (12)		0.0000 (13)	
E_{22223}	1.1 (2)		2.8 (3)		3.9 (5)		5.5 (6)	
E_{22333}	-0.002 (4)		0.002 (6)		0.000 (10)		0.007 (12)	
E_{33333}	-0.0005 (4)		0.0004 (6)		0.0010 (10)		0.0005 (12)	

* Third-order tensor elements C_{pqr} are multiplied by 10^5 . Fourth-order tensor elements D_{pqrs} are multiplied by 10^6 . Fifth-order tensor elements E_{pqrst} are multiplied by 10^7 .

Schulz, 1984). It is clear that the Ag2 site presents lower displacement parameters (higher value for the maximum of density) than the Ag1 site. For this reason, the expansion was limited to the third order for this site. One section of the Ag1 non-harmonic deformation-density map (Kuhs, 1988) is plotted in Fig. 3. A good agreement is found between the non-harmonic contribution to the density function and the major residues of the harmonic model (Fig. 1a). The

results for this final model have been compiled in Tables 2, 3 and 4.

To unravel the origin of the silver density deformation, a temperature dependence analysis of the silver distribution was initiated (Bachmann & Schulz, 1984). The model that was found for the room-temperature structure was taken as a starting point for the three high-temperature data set refinements. No critical departures from the initial model were noticed. The following

R/wR values of 0.0354/0.0363, 0.0399/0.0495 and 0.0390/0.0378 were obtained for the data sets collected at 348, 398 and 448 K, respectively. The final parameters for Ag are compiled in Table 4, the parameters for the other atoms can be obtained upon request.*

3. Discussion

A stereoscopic view of the $\text{Ag}_2\text{Ti}_2\text{P}_2\text{S}_{11}$ layered structure is presented in Fig. 4. The layers, perpendicular to the c axis, can conveniently be described in terms of $[\text{Ti}_2\text{S}_9]$ chains running along the b direction. The chains have no atom in common, but are linked through an intricate network of corner-sharing $[\text{AgS}_4]$ and $[\text{PS}_4]$ tetrahedra. This latter network is rather compact and defines a uniform slab of almost constant thickness, which constitutes the central part of the layers. The $[\text{Ti}_2\text{S}_9]$ chains are grafted alternatively on both sides of that slab, giving the layer its puckered aspect. The layers stack in an efficient way, with a perfect matching of the undulations maximizing the van der Waals interactions across the gaps.

A $[\text{Ti}_2\text{S}_9]$ chain is presented in Fig. 5, along with the $[\text{AgS}_4]$ and $[\text{PS}_4]$ polyhedra that take part in its connection to the layer and, therefore, to the neighbouring chains. This $[\text{Ti}_2\text{S}_9]$ chain can be considered as an edge-sharing chain of $[\text{TiS}_6]$ octahedra, in which one of the two S atoms of every other edge has been replaced by an S_2 group. Such polyhedra are referred to as G1 in the Evain & Brec (1992) classification. The S—S distance of the S_2 group, 2.034 (2) Å, is characteristic of the usual $(\text{S}_2)^{2-}$ pair (important interatomic distances

and angles are gathered in Table 5). Within the $[\text{TiS}_7]$ unit, the Ti atoms are off-centred, displaced towards the van der Waals gap. The reason is twofold: (i) the Ti atom moves away from the P and Ag atoms (*vide infra*) and (ii) the transition metal makes shorter bonds with the S atoms not involved in the $[\text{AgS}_4]$ and $[\text{PS}_4]$ entities. Indeed, the shortest Ti—S bond [2.3127(14) Å] is made with the lone S atom (S9, in front in Fig. 5) and the second shortest [2.459(2) Å] bond with the S_2 pair. However, the average Ti—S distance [2.493(2) Å] compares well with the 2.42 Å observed in TiS_2 (Ofteidal, 1928). The presence of the S_2 pair in every other titanium polyhedron connection leads to two different Ti—Ti distances along the $[\text{Ti}_2\text{S}_9]$ chain: 3.3585(13) and 3.4774(13) Å, the shorter distance corresponding to the coupling including the pair. These Ti—Ti distances ($d_{av} = 3.42$ Å) are comparable to the distance of 3.40 Å found in TiS_2 . The S_2 pair is also at the origin of the twofold superstructure along the c axis, since it imposes a shift of the layers along the b direction to achieve a better stacking of the slabs (see Fig. 4).

The P atoms are in almost regular tetrahedra with three coordinating atoms belonging to the $[\text{Ti}_2\text{S}_9]$ chain. However, a thorough analysis of the P—S distances and of the S—P—S angles reveals that the P atoms (P1 and P2) are slightly displaced from the tetrahedron centres, away from the Ti atoms.

The $[\text{AgS}_4]$ tetrahedra share two S atoms with two $[\text{TiS}_7]$ units of a $[\text{Ti}_2\text{S}_9]$ chain. Those two S atoms are also part of two different $[\text{PS}_4]$ groups, therefore, making a corner-sharing chain of alternating $[\text{AgS}_4]$ and $[\text{PS}_4]$ tetrahedra, parallel to the $[\text{Ti}_2\text{S}_9]$ chain (see Fig. 5). In each $[\text{AgS}_4]$ tetrahedron, the length of the S—S edge parallel to the chain is imposed by the periodicity of the $[\text{Ti}_2\text{S}_9]$ chain. These distances are 3.476(2) and 3.384(2) Å for Ag1 and Ag2, respectively, that is,

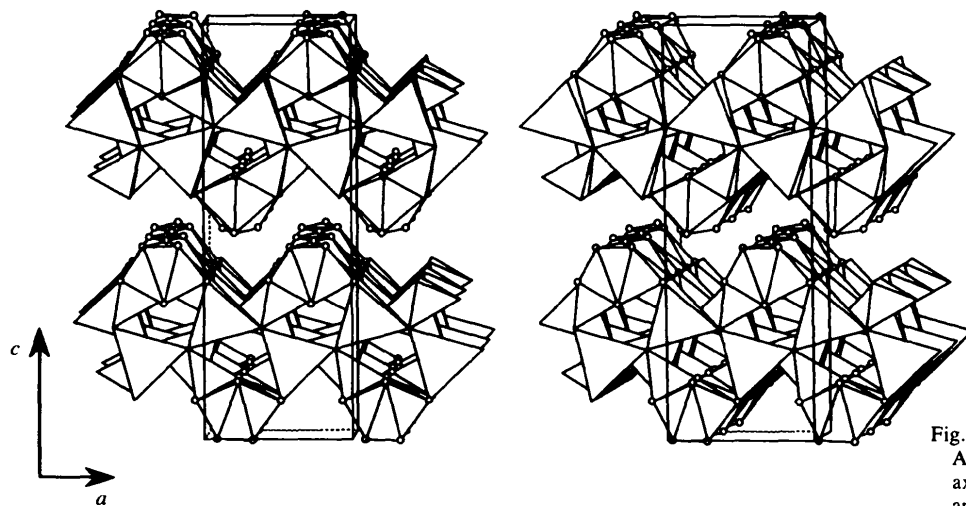


Fig. 4. Stereoscopic view of the $\text{Ag}_2\text{Ti}_2\text{P}_2\text{S}_{11}$ structure along the b axis showing its layered nature and overall arrangement.

*A list of structure factors has been deposited with the IUCr (Reference: DU0410). Copies may be obtained through The Managing Editor, International Union of Crystallography, 5 Abbey Square, Chester CH1 2HU, England.

Table 5. Main interatomic distances (Å) and angles (°)†

AgS ₄ sites			
Ag1*—S1	2.558 (3)	Ag1*—S3 (×2)	2.834 (3)
Ag1*—S1	2.633 (3)	Ag1*—Ag1	0.065
Ag1*—S _{av}	2.715 (3)		
(S1—Ag1*—S1)	117.61 (11)	(S1—Ag1*—S3)	112.32 (8)
(S3—Ag1*—S3)	75.67 (7)	(S1—Ag1*—S3)	115.95 (8)
Ag2*—S2	2.589 (3)	Ag2*—S4 (×2)	2.736 (2)
Ag2*—S2	2.665 (3)	Ag2*—Ag2	0.054
Ag2*—S _{av}	2.682 (3)		
(S2—Ag2*—S2)	114.57 (8)	(S2—Ag2*—S4)	115.03 (6)
(S4—Ag2*—S4)	76.40 (6)	(S2—Ag2*—S4)	115.24 (6)
PS ₄ sites			
P1—S1	2.012 (3)	P1—S4 (×2)	2.042 (2)
P1—S5	2.078 (3)		
P1—S _{av}	2.045 (3)		
(S1—P1—S4)	112.45 (8)	(S4—P1—S4)	115.38 (11)
(S1—P1—S5)	112.62 (12)	(S4—P1—S5)	101.44 (8)
P2—S2	2.009 (3)	P2—S3 (×2)	2.039 (2)
P2—S6	2.068 (3)		
P2—S _{av}	2.041 (3)		
(S2—P2—S3)	113.75 (8)	(S3—P2—S3)	110.93 (11)
(S2—P2—S6)	114.90 (12)	(S3—P2—S6)	101.09 (8)
TiS ₇ site			
Ti—S3	2.516 (2)	Ti—S7	2.468 (2)
Ti—S4	2.619 (2)	Ti—S8	2.459 (2)
Ti—S5	2.535 (2)	Ti—S9	2.3127 (14)
Ti—S6	2.5399 (14)		
Ti—S _{av}	2.493 (2)		
S7—S8	2.034 (2)		

† Positions with a star superscript refer to the Ag1* [0.3996 (2), 0.25, 0.30394 (10)] and Ag2* [0.6054 (2), 0.75, 0.19283 (6)] mode positions ($T = 293$ K).

much smaller than the average S—S distance of 4.34 Å calculated for the [AgS₄] tetrahedra. As a result, the [AgS₄] tetrahedra are extremely flattened along the *b* direction. The tetrahedron skewing is slightly different for the two Ag atoms, because of their relative positions with regard to the S₂ pairs. This last observation explains the difference in ADP's of the two Ag atoms (*vide infra*). Both Ag atoms are off-centred in a similar

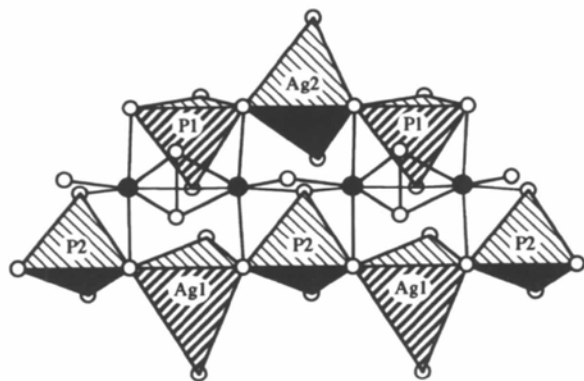


Fig. 5. The [Ti₂S₉] chain and its connections to the [AgS₄] and [PS₄] units. Ti and S atoms as full and open circles, respectively.

way to the P atoms, to reduce the Ag—Ti interaction. This leads to one longer, two average and one shorter Ag—S distances per tetrahedron, the overall Ag—S average distance (2.70 Å) being identical to that found in Ag₄P₂S₆, for instance (Tofoli, Khodadad & Rodier, 1983). With the usual oxidation state for Ag, Ti and P and taking into account the S₂ pair, a straightforward

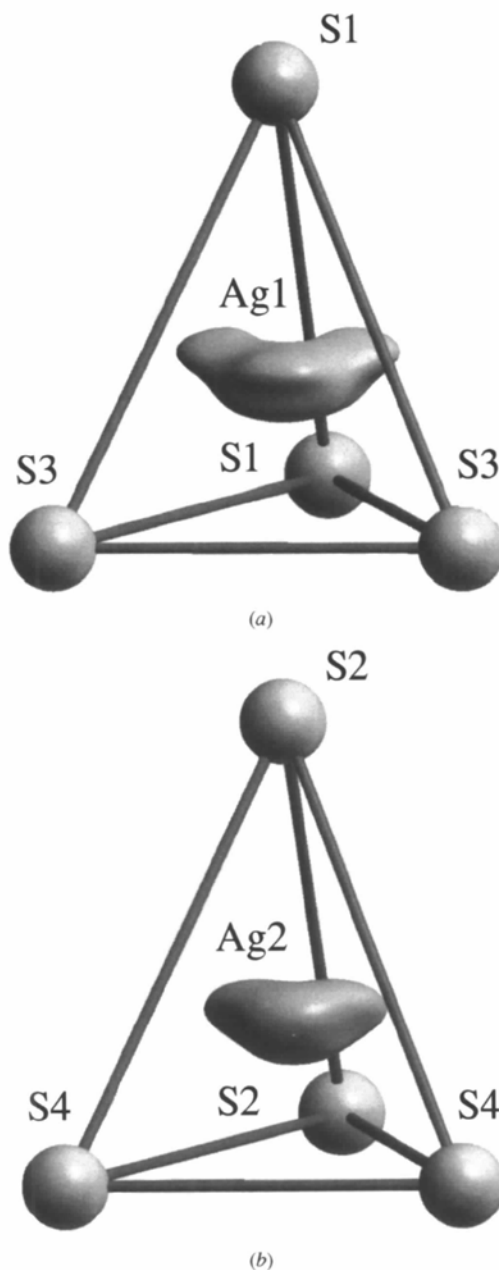


Fig. 6. Three-dimensional representations of silver probability density surfaces at 293 K for the (a) Ag1 and (b) Ag2 tetrahedra, indicating a smearing of the density towards two equivalent faces: S atoms are represented as spheres of arbitrary size.

charge balance, $\text{Ag}_2^{\text{I}}\text{Ti}_2^{\text{IV}}\text{P}_2^{\text{V}}(\text{S}_2)^{-\text{II}}\text{S}_9^{-\text{II}}$, can be established.

Room-temperature silver probability density surfaces are presented in Figs. 6(a) and (b) for Ag1 and Ag2, respectively. Clearly, the probability density deformation increases the electron density towards the tetrahedron faces that are not parallel to the skewing direction, that is, the faces that have not been reduced in size in the flattening process. The deformation is more pronounced for Ag1 than for Ag2. This latter observation is to be related to the different positions of the Ag atoms along the $[\text{Ti}_2\text{S}_9]$ chain and, therefore, to the different sizes and distortions of the Ag1 and Ag2 tetrahedra. Silver mode positions are calculated to be

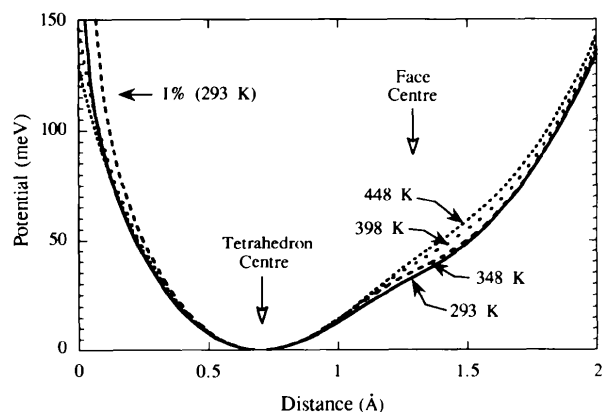


Fig. 7. The effective one-particle potential of Ag1 along a direction from the mode position (in the tetrahedron centre vicinity) towards the maximum of p.d.f. within one of the two equivalent $[\text{S}1, \text{S}1, \text{S}3]$ faces (see Fig. 6a). The 1% significance limit, according to Boltzmann statistics, is indicated for $T = 293 \text{ K}$.

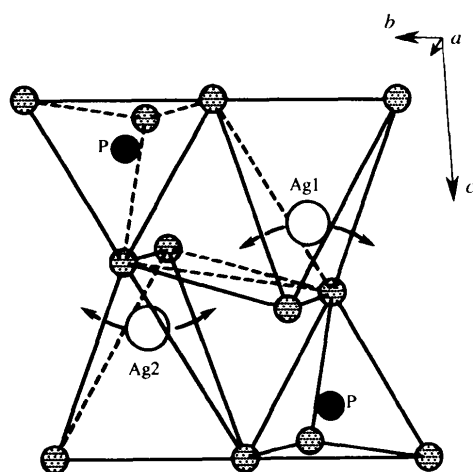


Fig. 8. The silver distribution as a function of temperature: At high temperature the tetrahedrally coordinated site is the preferential site. At lower temperature the Ag atoms are redistributed over the tetrahedral site and the adjacent triangular site, towards neighbouring empty tetrahedra.

displaced by *ca* 0.06 Å from the mean positions (see Table 5). To determine the origin of the non-harmonical behaviour of silver – anharmonicity or positional disorder – a temperature-dependent study was carried out (*vide supra*). Fig. 7 presents the effective one-particle potential of Ag1 along the direction going from the Ag1 mode position towards the maximum of p.d.f. within one of the two equivalent $[\text{S}1, \text{S}1, \text{S}3]$ tetrahedron faces. A clear deformation is observed upon lowering the temperature from 448 K to room temperature, with a maximum effect outside the tetrahedron, close to the sulfur triangular face. This change of potential curvature as a function of temperature is characteristic of a statistically disordered structure (Bachmann & Schulz, 1984). At high temperature the tetrahedrally coordinated site is the preferential site. At lower temperature the Ag atoms are redistributed over the tetrahedral site and the adjacent triangular site. The triangular faces are possible sites for Ag atoms since the adjacent tetrahedra are empty, with their centres not too close to the neighbouring P atoms, as illustrated in Fig. 8. No sign of ionic conductivity could be detected, that is no density was found between the Ag atoms. However, this does not preclude an ionic conductivity (conductivity measurements will be carried out when a pure sample will be available), although it is unlikely due to the large separation between the Ag atoms (*ca* 4.6 Å) and the short S—S edge (*ca* 4.1 Å, see Fig. 8) they would have to go through (notice that the usual Ag—S separation for Ag atoms in linear sulfur coordination is *ca* 2.4 Å).

The silver behaviour observed in $\text{Ag}_2\text{Ti}_2\text{P}_2\text{S}_{11}$ is similar to a previous observation made for $\text{Ag}_2\text{MnP}_2\text{S}_6$ (van der Lee, Boucher, Evain & Brec, 1993). Indeed, the Ag atoms are observed to move from a lower coordination (triangular) to a higher coordination (tetrahedral) upon increasing the temperature. However, in $\text{Ag}_2\text{MnP}_2\text{S}_6$ the positions are resolved but they are not in $\text{Ag}_2\text{Ti}_2\text{P}_2\text{S}_{11}$, even at the lowest temperature of the analysis (see Fig. 7). To see if the silver disorder could be resolved below room temperature for $\text{Ag}_2\text{Ti}_2\text{P}_2\text{S}_{11}$, new data collections were initiated. They could not be properly carried out, however, because of a reversible phase transition at *ca* 228 K, occurring with a splitting of spots probably related to a twinning of the structure upon ordering. Complementary studies to analyse that transition are under way.

4. Conclusions

The formula of the new compound can be written as $\text{Ag}_2^{\text{I}}\text{Ti}_2^{\text{IV}}\text{P}_2^{\text{V}}(\text{S}_2)^{-\text{II}}\text{S}_9^{-\text{II}}$. The structure is composed of layers, separated by van der Waals gaps. The $\text{Ag}_2\text{Ti}_2\text{P}_2\text{S}_{11}$ slabs are made of $[\text{Ti}_2\text{S}_9]$ chains built from $[\text{TiS}_7]$ units and linked through $[\text{PS}_4]$ and $[\text{AgS}_4]$ tetrahedra. An anharmonic development of the atomic displacement factor for Ag atoms reveals a strong non-harmonical p.d.f. deformation, especially in the direction

of two empty neighbouring tetrahedra, away from the Ti and P cations. An analysis of the effective one-particle potential as a function of temperature suggests a statistically disordered structure. However, the disorder could not be resolved at low temperature, because of a phase transition with splitting of spots just below room temperature.

References

- Bachmann, R. & Schulz, H. (1984). *Acta Cryst.* **A40**, 668–675.
- Barj, M., Lucazeau, G., Ouvrard, G. & Brec, R. (1988). *Eur. J. Solid State Inorg. Chem.* **25**, 449–461.
- Becker, P. J. & Coppens, P. (1974). *Acta Cryst.* **A30**, 129–147.
- Boucher, F. (1993). Thèse de doctorat. Université de Nantes.
- Boucher, F., Evain, M. & Brec, R. (1994). *J. Alloys Compd.* **215**, 63–70.
- Brec, R. (1986). *Solid State Ion.* **22**, 3–30.
- Burdett, J. K. & Eisenstein, O. (1992). *Inorg. Chem.* **31**, 1758–1762.
- Cieren, X., Angenault, J., Couturier, J.-C. & Quarton, M. (1995). Vth European Conference on Solid State Chemistry, 4–7 September. Montpellier, France.
- Cromer, D. T. (1974). *International Tables for X-ray Crystallography*, Vol. IV, pp. 149–150. Birmingham: Kynoch Press. (Current distributor Kluwer Academic Publishers, Dordrecht.)
- Cromer, D. T. & Waber, J. T. (1974). *International Tables for X-ray Crystallography*, Vol. IV, pp. 72–98. Birmingham: Kynoch Press. (Present distributor Kluwer Academic Publishers, Dordrecht.)
- Durand, E., Evain, M. & Brec, R. (1993). *J. Solid State Chem.* **102**, 146–155.
- Durand, E., Ouvrard, G., Evain, M. & Brec, R. (1990). *Inorg. Chem.* **29**, 4916–4920.
- Evain, M. & Brec, R. (1992). *Struct. Bonding*, **79**, 277–306.
- Friedel, C. R. (1894). *C. R. Acad. Sci.* **119**, 260–264.
- Hall, S. R., King, G. S. D. & Stewart, J. M. (1995). Editors. *XTAL3.4 User's Manual*. Universities of Western Australia, Australia, and Maryland, USA.
- Jandali, W. M. J., Eulenberger, G. & Hahn, H. (1980). *Z. Anorg. Allg. Chem.* **470**, 39–44.
- Jandali, W. M. J., Eulenberger, G. & Hahn, H. (1985). *Z. Anorg. Allg. Chem.* **530**, 144–154.
- Jansen, M. (1987). *Angew. Chem. Int. Ed. Engl.* **26**, 1098–1110.
- Johnson, C. K. & Levy, H. A. (1974). *International Tables for X-ray Crystallography*, Vol. IV, pp. 311–336. Birmingham: Kynoch Press. (Present distributor Kluwer Academic Publishers, Dordrecht.)
- Klingen, W., Eulenberger, G. & Hahn, H. Z. (1968). *Naturwissenschaften*, **55**, 229–230.
- Kuhs, W. F. (1984). *Acta Cryst.* **A40**, 133–137.
- Kuhs, W. F. (1988). *Aust. J. Phys.* **41**, 369–382.
- Lee, A. van der, Boucher, F., Evain, M. & Brec, R. (1993). *Z. Krist.* **203**, 247–264.
- Lee, S., Colombet, P., Ouvrard, G. & Brec, R. (1986). *Mater. Res. Bull.* **21**, 917–928.
- Oftedal, I. (1928). *Z. Phys. Chem.* **134**, 301–310.
- Ouvrard, G. & Brec, R. (1988). *Mater. Res. Bull.* **23**, 1199–1209.
- Ouvrard, G., Fréour, R., Brec, R. & Rouxel, J. (1985). *Mater. Res. Bull.* **20**, 1053–1062.
- Petricek, V. (1995). *SDS95*. Institute of Physics, Praha, Czech Republic.
- Tofoli, P., Khodadad, P. & Rodier, N. (1983). *Acta Cryst.* **C39**, 1485–1488.
- Sheldrick, G. M. (1991). *SHELXTL-Plus*. Release 4.1. Siemens Analytical X-ray Instruments Inc., Madison, Wisconsin, USA.
- Yoshiasa, A., Koto, K., Kanamaru, F., Emura, S. & Horiuchi, H. (1987). *Acta Cryst.* **B43**, 434–440.
- Zhukov, V., Boucher, F., Alemany, P., Evain, M. & Alvarez, S. (1995). *Inorg. Chem.* **34**, 1159–1163.